Journal of Materials Chemistry A

Dual functionality of over-lithiated NMC for high energy silicon-based lithium-ion batteries

Journal:	*Journal of Materials Chemistry A*
Manuscript ID	TA-ART-02-2021-001290.R1
Article Type:	Paper
Date Submitted by the Author:	12-Mar-2021
Complete List of Authors:	Dose, Wesley ; Argonne National Laboratory, Chemical Sciences and Engineering Division kim, soojeong; Argonne National Laboratory, Chemical Sciences and Engineering Division Liu, Qian; Argonne National Laboratory Trask, Stephen; Argonne National Laboratory, Chemical Sciences and Engineering - Electrochemical Energy Storage Dunlop, Alison; Argonne National Laboratory, Chemical Sciences and Engineering Division Ren, Yang; Argonne National Laboratory Zhang, Zhengcheng; Argonne National laboratory, Chemical Engineering Division Fister, Tim; Argonne National Laboratory, Chemical Sciences and Engineering Johnson, Christopher; Argonne National Laboratory, Chemical Sciences and Engineering Division

Dual functionality of over-lithiated NMC for high energy silicon-based lithium-ion batteries

Wesley M. Dose[z,*], Soojeong Kim, Qian Liu, Stephen E. Trask, Alison R. Dunlop, Yang Ren, Zhengcheng Zhang, Timothy T. Fister, Christopher S. Johnson[z]

Chemical Sciences and Engineering Division, Argonne National Laboratory, Lemont, Illinois, U.S.A. 60439.

[z] Correspondence: wmd23@cam.ac.uk, cjohnson@anl.gov

* Current address:
Department of Chemistry, University of Cambridge, Lensfield Road, Cambridge, CB2 1EW, Cambridge, UK.
Department of Engineering, University of Cambridge, 17 Charles Babbage Road, CB3 0FS, Cambridge, UK.

Abstract

Owing to their high specific capacity and suitably low operating potential, silicon-based anodes are an attractive alternative to graphite in next-generation lithium-ion batteries. However, silicon anodes suffer from low initial coulombic efficiency and fast capacity decay, limiting their widespread application. Pre-lithiation strategies are highly appealing to compensate for irreversible active lithium loss and to boost the cell energy density. In this work, we maximize the cell energy density by direct pre-lithiation of the NMC ($LiNi_{0.5}Mn_{0.3}Co_{0.2}O_2$) cathode to $Li_{1+x}NMCO_2$ without introducing inactive deadweight to either electrode. First, we demonstrate that $Li_{1+x}NMCO_2$ can be synthesized chemically, via reaction between NMC and lithium napthalide, and electrochemically. The NMC cathode is tolerant of a one-time over-lithiation up to 60 mAh g^{-1}_{NMC}, giving capacity retention on par with untreated NMC in half cell electrochemical cycling. Using synchrotron X-ray absorption spectroscopy (ex situ) and diffraction (in situ), we demonstrate that higher amounts of over-lithiation lead to local structure distortion – driven by transition metal reduction to Jahn-Teller active Mn^{3+} and Co^{2+} – as well as

bulk structural hysteresis during over-lithiation and layer "buckling" that increases the amount of lithium extracted from the structure in the charged state. The $Li_{1+x}NMCO_2$ with low-to-moderate over-lithiation capacity (23, 46, and 70 mAh g^{-1}_{NMC}) is proven to be a highly effective dual-purpose lithium source and cathode material in full cell tests with a commercially relevant Si-graphite anode. These cells show higher capacity, superior cycle life, and improved coulombic efficiencies when compared to those with stoichiometric NMC cathodes. This study introduces a new and simple method to pre-lithiate layered transition metal oxide cathodes, opening up new possibilities for the development of high energy density lithium-ion batteries with next-generation anodes.

Introduction

Progress in battery energy storage is driven by focused investigations of electrode failure that guides research towards strategies to resolve or mitigate the problem. Electrodes for lithium-ion batteries (LIBs) lose capacity and fail in a variety of ways. For example, layered transition metal oxides are the current forerunner cathode material for electric vehicles (EVs), owing to their high energy density and (de)intercalation stability. However, repeated charging to high voltages to access the full capacity is detrimental leading to energy fade.[1–5] Impedance increase from electrolyte decomposition, surface oxygen loss, phase transitions at the particle surface, and cracking at grain boundaries are largely responsible for the loss in cathode performance.[3,5–19] In addition, transition metal dissolution from the cathode is harmful to the graphite anode causing capacity loss due to lithium trapping.[4,20,21] Selecting an optimized material composition and voltage window for charge-discharge has proven successful in commercializing layered transition metal oxides in EV batteries, with $LiNi_{0.5}Mn_{0.3}Co_{0.2}O_2$ (NMC532) found in the current generation of some EVs.[10]

Potential next-generation anode materials for LIBs degrade in different ways compared to cathodes. One promising candidate is silicon, which is abundant, cheap, and environmentally benign. Silicon alloys with lithium to a theoretical electrochemical lithiation capacity of 3579 mAh g^{-1}.[22] However, the large first cycle irreversible capacity and rapid capacity fade are major drawbacks for the performance of this anode material.[23–26] Both problems are related to active lithium loss.[27–29] In the first lithiation of silicon, components of the electrolyte are reduced on the anode surface forming a solid electrolyte interphase (SEI). As lithiation progresses, the silicon particles continuously expand exposing fresh, unreacted surfaces that undergo further SEI passivation reactions. Consequently, a sizable fraction of the lithium ions delivered to the anode during the first charge of the full cell are immobilized in the SEI and are electrochemically inactive. Active lithium depletion in later cycles, a result of repeated particle expansion and contraction, together with silicon particle and electrode degradation, continue to cause energy loss (capacity decline) in silicon-containing cells.[23–26]

A common strategy to counteract the loss of lithium is to increase the amount of active lithium initially in the full cell. This has been demonstrated via an increasing number of methods (reviewed recently in ref.[30]). For example, anode pre-lithiation with stabilized Li powder,[31–33] anode electrochemical lithiation,[34–37] sacrificial lithium containing salts or lithium-rich solid-state compounds on the cathode or anode,[38–47] and chemical lithiation of the cathode or anode.[48–52] Two important considerations here are the method practicality and the extra weight added to the system. From a practical standpoint, pre-lithiation of anode materials via lithium metal powder or electrochemical lithiation is challenging owing to their air instability and high chemical reactivity, which cause compatibility issues during electrode manufacture.[45] For sacrificial lithium containing salts, residues are left in the electrode after lithium release,

lowering the gravimetric capacity and cell energy density.[45] For example, a nanoscale mixture of Co/Li_2O has been proposed as a pre-lithiation additive, delivering a capacity around 600 mAh g^{-1}.[38] But after lithium release, inactive Co_3O_4 remains on the cathode as deadweight. Direct pre-lithiation of the cathode active material circumvents both of the above pitfalls. In this work, we propose that moderately over-lithiated layered transition metal oxide, $Li_{1+x}MO_2$ with $x<0.5$, can act as both a lithium source and cathode material to increase the lithium inventory of the full cell – hence having dual-functionality.

Chemical and electrochemical over-lithiation of cathode materials has been studied since the early 1990s.[53] While much of the early research focused on lithiation of the $Li_{1+x}Mn_2O_4$ 4 V spinel,[53–56] Johnson et al.[57,58] first demonstrated over-lithiation of layered mixed transition metal oxides for $Li_2Ni_{0.5}Mn_{0.5}O_2$. (Li_2MnO_2[59] and Li_2NiO_2[60] had been synthesized in the 1980s and 1990s, respectively.) Since then most reports of $Li_{1+x}MO_2$ (where M is a combination of two or more transition metals) focus on (i) prospective high capacity cathodes cycling greater than one lithium ion per formula unit,[57,58] (ii) origins of first cycle irreversibility,[61,62] or recently (iii) the effect of over-discharge.[63,64] In contrast, in the present study we demonstrate that over-lithiated $Li_{1+x}MO_2$ cathodes can be used directly to increase the lithium inventory and energy density of a full cell with a Si-based anode. To investigate the effect of over-lithiation on NMC materials a NMC532 cathode is employed. This over-lithiated NMC cathode is successfully used to compensate for the lithium losses in $Li_{1+x}Ni_{0.5}Mn_{0.3}Co_{0.2}O_2$/Si-graphite full cells, resulting in a higher energy density and dramatically extending cycle life.

Experimental

Electrodes used in this work were supplied by the Cell Analysis Modeling and Prototyping (CAMP) facility at Argonne. The NMC532 positive electrode has a composition of

90 wt.% NMC532 (Toda), 5 wt.% C-45 conductive carbon, and 5 wt.% polyvinylidene fluoride (PVDF) as the binder. The Si-graphite negative electrode was prepared with a composition of 15 wt.% Si (Paraclete Energy Silicon), 73 wt.% graphite (Hitachi MagE3), 2 wt.% C-45 carbon, and 10 wt.% lithium polyacrylate (LiPAA) binder. Punched electrodes, 14 mm diameter for the NMC cathode and 15 mm diameter for the Si-graphite anode, were dried in a vacuum oven overnight at 75 °C and 150 °C, respectively. The loading of the cathode was 10.2(2) mg cm^{-2} (1.86(3) mAh cm^{-2}) and the anode was 2.8(2) mg cm^{-2} (2.80(1) mAh cm^{-2}).

Electrochemical measurements were performed in 2032-type coin cells that were assembled in an argon-filled glovebox with oxygen levels less than 1 ppm. Cells were built with 45 μL of electrolyte, which contains 1.2 M $LiPF_6$ in ethylene carbonate (EC): ethyl methyl carbonate (EMC) 3:7 by weight with 10 wt.% fluorethylene carbonate (FEC). The Celgard separator was dried at 60 °C under vacuum prior to use. Half cell measurements used 15.6 mm diameter lithium metal chips (MTI) as the reference/counter electrode. All electrochemical tests were performed at 30 °C using a MACCOR Series 4000 Test System. Half cell testing was conducted at C/10 (assuming a theoretical capacity of 180 mAh g^{-1}_{NMC}) and in a 3.0-4.5 V vs Li/Li^+ potential range for NMC532, and in a 0.01-1.5 V vs Li/Li^+ potential range for Si-graphite. Electrochemical lithiation of NMC532 was conducted in half cell configuration, where the cathode was discharged to a certain capacity (20, 40, 60, 80 and 100 mAh g^{-1}_{NMC}) or potential (1.1 V vs Li/Li^+) limitation. In the discharged state and in an argon filled glovebox the cell was decrimped. The lithiated cathode was extracted from the cell and immediately rebuilt in a $Li_{1+x}NMCO_2$/Si-graphite full cell. $Li_{1+x}NMCO_2$/Si-graphite full cell performance was evaluated in a 3.0-4.1 V potential window. The cycling protocol consisted of 100 cycles, made up of three C/20 formation cycles, 94 C/3 aging cycles, and three C/20 diagnostic cycles. The first and last

C/3 cycles applied a hybrid pulse power characterization (HPPC)[65] test on discharge to measure the DC impedance. At pre-determined cell voltages a 3 C, 10 s discharge pulse followed 40 s later by a 2.5 C, 10 s charge pulse was applied; at each voltage the cell was allowed to equilibrate for 1 h prior to the first 10 s pulse.

Ex-situ Ni, Co and Mn K-edge X-ray absorption spectroscopy (XAS) was performed to detect the change of the transmission metal valence states for pristine and over-lithiated cathodes at beamline 10BM (MRCAT) at the Advanced Photon Source (APS) at Argonne National Laboratory (Argonne). The measurements were carried out in transmission mode with a downstream Ni, Co, or Mn metal foil as a reference, which provides internal calibration for the X-ray energy. Coin cells with NMC532 as the cathode and Li metal as the anode were over-lithiated to 1.1 V vs Li/Li^+ using constant current mode. The cells were decrimped in an argon filled glove box and the cathode extracted. The electrodes were washed in 1 mL of dimethyl carbonate (DMC) to remove excess electrolyte, dried under vacuum at 70 °C, and sealed between two pieces of Kapton tape for measurement at the beam line. The X-ray absorption near edge structure (XANES) spectra were normalized and analyzed using the ATHENA software package.[66]

Cells for in situ synchrotron X-ray diffraction (XRD) measurements were constructed using modified 2032 coin cells with 2 or 3 mm diameter holes in the cell casing. NMC532 was used as the cathode and a lithium metal chip as the counter/reference electrode. To maintain stack pressure and conductivity, a 0.7 mm thick glassy carbon disk with a thinner 0.2 mm window in the center was employed on the cathode side. The cell was hermetically sealed by an O-ring (see schematic in Figure S1). On the counter electrode side a 0.5 mm thick glassy carbon disk maintained even stack pressure and the cell was sealed with an aluminized Kapton window.

The electrochemical protocol for the in situ cells was as follows: discharge at C/8 to a capacity (20, 40, 60, 80 and 100 mAh g^{-1}_{NMC}) or voltage (1.1 V vs Li/Li^+) limitation, charge to 4.5 V vs Li/Li^+, and discharge to 3.0 V vs Li/Li^+. Due to time constraints at the beam line the final discharge step did not complete for the larger over-lithiation capacity cells. The high energy synchrotron XRD measurements were carried out at beamline 11-ID-C at the APS (λ = 0.1173 Å). Scans were collected in a Debye-Scherrer geometry using an amorphous-Si PerkinElmer 1621 area detector with a 20 s exposure time and 8 min between scans. The data were integrated (0.25-9.25 °2θ, 0.002 °2θ step) using GSAS-II[67] using a CeO_2 standard (SRM674b) as calibrant. Background subtraction was performed based on the average of multiple scans collected for a cell with the glassy carbon windows, but without electrodes or electrolyte. The 2θ regions that include reflections from Li metal were excluded. Rietveld refinements were carried out using GSAS-II with a structural model based on the *R*-3*m* space group. During sequential refinements the refined parameters were the lattice parameters (a and c), scale factor, z position for O^{2-} and an isotropic strain term. Other parameters, such as the atomic displacement parameters and isotropic size were refined initially and then fixed.

NMC532 (Toda) was lithiated chemically using the procedure outlined in ref.[58]. In brief, NMC532 powder was stirred at room temperature for 4 days in a 50 % mole excess 0.1 M lithium naphthalide solution that had been freshly prepared from naphthalene (Alfa Aesar, 99.6 %) and metallic lithium (MTI) in tetrahydrofuran (THF; Aldrich ≥99.9 %) solvent. The product was filtered and washed in diethyl ether (Aldrich, ≥99.9 %) and stored in an argon glovebox (O_2 <1 ppm). The Li, Ni, Mn, and Co molar ratio was analyzed by using an inductively coupled plasma−mass spectrometer (ICP-MS, DRCII; PerkinElmer, Shelton, CT). The $Li_{1+x}NMCO_2$ powder was dissolved in concentrated HNO_3/HCl and diluted to the low ppb level for

measurement. The structure of $Li_{1+x}NMCO_2$ was confirmed by high energy synchrotron XRD at beamline 11-ID-C at the APS (λ = 0.1173 Å).

X-ray diffraction was used to assess the ambient environment stability of over-lithiated cathodes using a Rigaku Miniflex diffractometer with Cu Kα radiation (λ = 1.5406 Å). Samples were placed on a silicon zero diffraction plate with an amorphous carbon-based grease and measured between 10-80° 2θ with a 0.02° step size and 0.4 s per step.

Results and discussion

Over-lithiation of NMC

Galvanostatic cycling experiments with a lithium metal counter/reference electrode were performed to demonstrate the over-lithiation capacity of $Li_{1+x}Ni_{0.5}Mn_{0.3}Co_{0.2}O_2$ ($Li_{1+x}NMCO_2$), where x is the mole fraction of additional lithium. Typical charge-discharge potential profiles for $LiNMCO_2$ are shown in Figure 1a, where lithium is initially extracted from the layered structure. Figure 1a also shows, however, than upon an initial discharge $LiNMCO_2$ will accept an additional 127 mAh g^{-1}_{NMC} of capacity above 1.1 V vs Li/Li^+, yielding an over-lithiation composition of $Li_{1.46}NMCO_2$. Two stages are noted in the potential profile: Stage I, a short 20 mAh g^{-1}_{NMC} sloping potential region from 1.6-1.5 V vs Li/Li^+; and Stage II, a longer plateau at 1.5 V vs Li/Li^+ before the potential polarizes to 1.1 V vs Li/Li^+. A similar $Li_{1+x}NMCO_2$ composition is also realized if the lithiation to 1.1 V vs Li/Li^+ is preceded by delithiation of the cathode (Figure S2). Accessing the short, sloped region between 1.6-1.5 V vs Li/Li^+ has been shown to "recover" the irreversible capacity on the first charge-discharge cycle,[61,62] lost due to sluggish lithium diffusion kinetics.[68–70] Kang et al.[61,62] show that NMC111 cycled with 100 % coulombic efficiency has an end-of-discharge potential of ~1.5 V vs Li/Li^+ that gradually increases to ~3 V vs Li/Li^+ during a 20 h OCP relaxation period. This differs from the present

work where over-lithiation was performed by discharging first, thereby adding extra lithium (x>0) to the system. Consequently, after over-lithiation accessing only the 1.6-1.5 V vs Li/Li^+ sloped region, 20 mAh g^{-1}_{NMC}, the potential of the cell is 1.5 V vs Li/Li^+ and during a 12 h rest the OCP quickly stabilizes to only a slightly higher potential of 1.55 V vs Li/Li^+ (Figure 1b).

Electrochemical lithiation of NMC demonstrates that $Li_{1+x}NMCO_2$ may be a viable pre-lithiation source and cathode. However, for practicality and to meet today's battery industry manufacturing requirements, electrode materials should be synthesized chemically, rather than electrochemically. $LiNMCO_2$ can be reduced to $Li_{1+x}NMCO_2$ in the presence of a 0.1 M lithium naphthalide solution in tetrahydrofuran (THF), with x tunable by the amount of lithium available in solution. To demonstrate this synthetic method, we attempted to prepare the fully lithiated form – composition Li_2NMCO_2 – using a 50 % excess of lithium in the reaction. The synchrotron X-ray diffraction (XRD) pattern of the lithiated product (after washing) is shown in Figure 2. Reflections from two phases can be observed in the diffraction pattern, which can be indexed to unreacted Li_1NMCO_2 with space group *R*-3*m* and lithiated Li_2NMCO_2 with space group *P*-3m_1. From Rietveld refinement the phase fractions are 17.4(1) % and 82.6(4) %, respectively, yielding a composition of $Li_{1.83(1)}NMCO_2$. A comparison of the *R*-3*m* Li_1NMCO_2 and *P*-3m_1 Li_2NMCO_2 structures is provided in Figure S3. From this schematic it is evident that the layered framework is maintained during over-lithiation, suggesting a certain robustness of the layered structural motif. The XRD analysis reveals that despite the excess of lithium in the reaction, the transition to Li_2NMCO_2 is incomplete for NMC532. This may be related to the fact that there are reported Li_2MO_2 layered oxides where M = Mn[59] and Ni,[60] although the corresponding layered Li_2CoO_2 has not been formed chemically or electrochemically. From inductively coupled plasma – mass spectrometry (ICP-MS) the composition of the washed power

was determined to be $Li_{2.13(1)}NMCO_2$, which suggests more rigorous washing procedures are required to remove lithium salt impurities. The air stability of $Li_{1+x}NMCO_2$ is an important consideration for practical application; however, a detailed investigation of this is beyond the scope of this work. Our initial experiments suggest that the reactivity of pre-lithiated NMC materials in ambient environment is slow (Figure S4), and thus effective surface protection countermeasures may facilitate the practical application of these materials.

Electrochemical performance of $Li_{1+x}NMCO_2$

For $Li_{1+x}NMCO_2$ to be an ideal pre-lithiation source and cathode, the over-lithiation step should not adversely affect the electrochemical performance of the material. To identify the impact of over-lithiation on subsequent cycling, Li/NMC cells were first electrochemically lithiated to various capacity limits (20, 40, 60, 80, 100 mAh g^{-1}_{NMC} and 1.1 V vs Li/Li^+ (123 mAh g^{-1}_{NMC})) and then cycled between 3.0-4.5 V vs Li/Li^+. Figure 3a shows that the additional lithium inserted at 1.5 V vs Li/Li^+ is extracted between 1.6 and 2.0 V vs Li/Li^+, after which the cell potential increases rapidly to 3.5 V vs Li/Li^+. However, not all the lithium inserted at 1.5 V vs Li/Li^+ is recovered at potentials below 3 V vs Li/Li^+. Rather, irrespective of the over-lithiation capacity, only 61 % of the additional lithium is extracted below 3 V vs Li/Li^+ implying significant potential hysteresis in the insertion-removal process. The discharge capacity for 50 cycles at C/10 between 3.0-4.5 V vs Li/Li^+ is shown in Figure 3b. Compared to the baseline without over-lithiation, lower extents of lithiation (20 and 40 mAh g^{-1}_{NMC}) show a small decrease in the delivered capacity, with similar rates of capacity fade. Conversely, ≥60 mAh g^{-1}_{NMC} of over-lithiation has led to greater rates of capacity fade, particularly over the first 20 cycles.

To understand the poor capacity retention after over-lithiation, the cathode state of charge (SOC) in the first cycle, or z in Li_zNMCO_2 (where z is used henceforth to be the total lithium

content), and the coulombic efficiency in the first two cycles are considered in Figure 3c and d, respectively. These are plotted as a function of the over-lithiation capacity. Firstly, over-lithiation to 20 and 40 mAh g^{-1}_{NMC} have resulted in similar, or slightly lower, degrees of lithium extraction at the end of the first charge to 4.5 V vs Li/Li^+. Higher over-lithiation led to a higher SOC at 4.5 V vs Li/Li^+, leaving proportionally less lithium in the layers. It is well established that cycling NMC to higher SOC, typically by cycling to higher voltages, is detrimental to the capacity retention. This is generally attributed to a combination of electrolyte oxidation, structural changes at the surface of the particle, and transition metal dissolution, causing an impedance rise on the cathode and capacity decline.[3–6,12–21] While the poor capacity retention noted here is consistent with prior reports, it does not explain why initial over-lithiation has led to greater degrees of lithium removal when using the same potential termination. In addition, consideration of the coulombic efficiency for the first and second cycles (Figure 3d, corrected in the first cycle by subtracting the over-lithiation capacity from the charge capacity) shows poorer reversibility for higher over-lithiation capacities. A similar trend is evident in the second cycle efficiencies, highlighting an issue with the ongoing reversibility. In the following section, ex situ X-ray absorption spectroscopy (XAS) is used to understand the transition metal oxidation state and local structure change after over-lithiation. Further, in situ synchrotron XRD is employed to gain insight into the bulk structural changes during over-lithiation and in the first charge-discharge cycle. Particularly, does the structural evolution indicate how over-lithiation has resulted in greater lithium removal at 4.5 V vs Li/Li^+ and a lower reversible capacity?

Synchrotron X-ray absorption spectroscopy and in situ X-ray diffraction

X-ray absorption near edge structure (XANES) spectra for the pristine NMC (0 mAh g^{-1}_{NMC} over-lithiation) and after over-lithiation to 1.1 V vs Li/Li^+ (123 mAh g^{-1}_{NMC}) at the Mn, Co

and Ni K-edge are shown in Figure 4a-c. The negative energy shift in the XANES is consistent with the reduction of each transition metal during discharge. Comparison of the main edge position with metal oxide standards indicates that the Mn oxidation state lies between 3+ and 4+ while the Co and Ni oxidation states are between 2+ and 3+ for the over-lithiated NMC, which is feasible for the $Li_{1.46}NMCO_2$ composition calculated from the electrochemistry. A strong increase in local disorder can also be seen in the Fourier transform of the extended X-ray absorption fine structure (EXAFS) of each metal species (Figure 4d-f). The Mn and Co show changes in metal-oxygen coordination as both ions become Jahn-Teller active at these conditions. In all cases, including the nickel sites, the second shell (metal-metal) coordination is affected by these distortions.

Synchrotron XRD scans collected during over-lithiation, delithiation (charge to 4.5 V vs Li/Li^+) and relithiation (discharge to 3.0 V vs Li/Li^+) at a C/8 rate are shown in Figure 5. Data was collected for all over-lithiation conditions, 20, 40, 60, 80, 100 mAh g^{-1}_{NMC} and to 1.1 V vs Li/Li^+, although for clarity only scans from the 20 mAh g^{-1}_{NMC} and 1.1 V vs Li/Li^+ cells are shown in Figure 5a and b, respectively. During Stage I (Figure 5a and b) the (003), (101), and (113) Bragg reflections (indexed based on the rhombohedral crystal system with *R*-3*m* space group) initially show a subtle shift in position to smaller angles. This is indicative of a solid solution lithium intercalation reaction, and expansion of the unit cell in the a and c directions. As over-lithiation proceeds into stage II (Figure 5b only), a two-phase reaction is evident. The intensity of reflections from the *R*-3*m* phase decrease and a new reflection at 1.31 °2θ (5.14 Å d-spacing, assigned to the (001) reflection of the Li_2NMCO_2 phase with $P\text{-}3m_1$ space group, and previously observed in other over-lithiated layered materials[57–60,63,71]) appears and grows in intensity. At 1.1 V vs Li/Li^+ this reflection remains weak, broad, and co-exists with *R*-3*m* phase

reflections, indicative of a disordered *P*-3m_1 structure in some electrode regions. Entering the two-phase region on over-lithiation leads to structural hysteresis on delithiation, with stage I-like structural behavior preceding stage II-like behavior. This is particularly evident in the lattice parameter evolution shown in Figure 6, which shows that while the structural changes on over-lithiation are reversible, they follow unique pathways on over-lithiation and delithiation. There is clearly a significant over-potential associated with lithium extraction from the Li_2NMCO_2 *P*-3m_1 phase. This is consistent with the hysteresis noted earlier in the potential profile, with 39 % of the over-lithiation capacity extracted at potentials higher than 3.0 V vs Li/Li^+. Conversely, over-lithiation to 20 mAh g^{-1}_{NMC}, only accessing stage I, shows structural reversibility without hysteresis.

Over-lithiation has affected the structural evolution on further delithiation to 4.5 V vs Li/Li^+ and relithiation to 3.0 V vs Li/Li^+ in three ways. Firstly, upon return to z=1 after over-lithiation the c lattice parameter is, on average, larger than the pristine material (Figure 6c and magnified in Figure S5 – in Figure S5 data for the 20 mAh g^{-1}_{NMC} and 100 mAh g^{-1}_{NMC} cells are compared). This suggests a structural memory effect from over-lithiation, likely related to a buckling of the close-packed oxygen array. Transitioning from *R*-3*m* (O3) to *P*-3m_1 (O1) requires the gliding of oxygen planes from cubic-close-packed (ccp) to hexagonal-close-packed (hcp). Irreversibility of this type of structural transformation has been reported for over-lithiation of $Li(Mn_{0.46}Ni_{0.46}Ti_{0.05}Li_{0.02})O_2$,[57] as well as for the O3 to O1 phase transition for $LiCoO_2$[72] and NMC111[73] that takes place in the highly charged state. Partial irreversibility of this phase change leaves stacking faults in the crystal lattice that may yield sites less stable to lithium occupation,[72] and/or disrupt lithium ion diffusion pathways. Second, high degrees of over-lithiation change the c lattice behavior at high SOC. Typically, for $0.45<z<1$ the c lattice parameter increases due to

increased electrostatic repulsion between basal and upper oxygen planes of adjacent transition metal-oxygen layers. Beyond z=0.45 the c lattice parameter decreases, attributed to charge transfer between O 2p and partially filled Ni e_g orbitals resulting in a decrease of oxygen-oxygen repulsion.[74] After high over-lithiation capacity, however, the c lattice parameter decrease is slowed, leaving a larger c lattice parameter, and hence inter-layer spacing, for a given SOC (Figure 6c and magnified in Figure S5f). A strong correlation between the c lattice parameter and the lithium ion diffusion kinetics has been reported in the literature.[75,76] Therefore, the larger inter-layer distance may facilitate faster lithium ion diffusion kinetics at high SOC, and hence a greater degree of lithium removal below 4.5 V vs Li/Li^+, as was noted in half-cells tests in Figure 3c. Thirdly, the greater degree of lithium removal (higher SOC) yields a smaller c lattice parameter in the fully charged state (Figure 6c and magnified in Figure S5f). The overall volume change in the charge-discharge cycle is therefore greater after high capacity over-lithiation. Previous studies have shown that cycling layered oxide cathodes to high SOC (larger volume changes) alters the particle microstructure, inducing microcracking.[7–9] It also leads to substantial structural changes at the particle surface, involving oxygen loss, transition metal reduction, site-mixing, and spinel/rock-salt phase formation, culminating in impedance rise.[3–6,12–21] Finally, the poorer structural reversibility after high capacity over-lithiation (see the (de)lithiation pathway differences in the a and c lattice parameters in Figure 6b and c and magnified in Figure S5g and h) reinforces that over-lithiation has permanently altered the crystal structure, possibly through structural inhomogeneity and inactive domains. Conversely, lower over-lithiation capacities lead to less severe reversibility issues, particularly when only the stage I solid-solution capacity (≤20 mAh g^{-1}_{NMC}) is accessed. We believe that developing new strategies to stabilize the NMC structure to over-lithiation will be a promising approach to improve these materials. Overall, our

investigation thus far has demonstrated that $Li_{1+x}NMCO_2$ is a viable lithium source for lithium inventory. At the same time this over-lithiated form itself acts as a fully functioning active cathode material, but only if the over-lithiation capacity is not too large.

$Li_{1+x}NMCO_2$/Si-graphite full cell evaluation

In this work, a Si-graphite composite electrode with 15 wt.% silicon and 73 wt.% graphite is used as the anode and paired with over-lithiated NMC cathodes in full cells; further details can be found in the experimental section. The addition of 15 wt.% silicon to the anode more than doubles the specific capacity over that of graphite alone, while the inclusion of graphite is intended to buffer the large volume changes of the silicon and provide better electrode electronic conductivity and stability than silicon alone. Representative half cell cycling data for this electrode is shown in Figure S6, revealing a first cycle lithiation capacity of 1024 mAh $g^{-1}_{Si\text{-}graphite}$, reversible capacity of 929 mAh $g^{-1}_{Si\text{-}graphite}$ and coulombic efficiency of 90.7 % when cycled at C/10 between 0.01-1.5 V vs Li/Li^+ (averages of two cells are quoted).

In a full cell, the lithium irreversibly consumed by the anode (SEI formation) on the first cycle reduces the amount of cyclable lithium. The amount of additional capacity required to refill the cathode (accounting for the irreversible capacity of NMC) was calculated based on the first charge-discharge cycle of a NMC/Si-graphite full cell; a representative potential profile is shown in Figure S7). The details of this calculation are given in supplementary note S1, and shows that the first cycle irreversible capacity due to lithium loss is 23.1 mAh g^{-1}_{NMC} for this Si-graphite electrode. Over-lithiation of NMC to 23 mAh g^{-1}_{NMC} is only marginally greater than the 20 mAh g^{-1}_{NMC} limit used in the half cell and in situ XRD experiments described above, which showed good capacity retention and structural reversibility. Two other over-lithiation amounts were examined as part of this study. The highest amount was designed to completely lithiate the

anode, leaving a safe margin to prevent lithium plating, and was calculated to be 70 mAh g^{-1}_{NMC} (details in supplementary note S2). This condition has the advantage of adding maximum lithium inventory to the cell. However, this is somewhat offset by the poorer cathode capacity retention due to higher NMC over-lithiation (Figure 3). Given the severity of the rate of lithium loss for silicon anodes, we anticipate that the silicon electrode will consume lithium at a faster rate than the over-lithiated NMC will lose available lithium sites. Therefore, capacity fade will be a function of the rate of lithium loss and the degradation of the active particles within the Si-graphite electrode. A third over-lithiation condition, between 23 and 70 mAh g^{-1}_{NMC}, of 46 mAh g^{-1}_{NMC} was also examined. Details of the NMC cathode and Si-graphite anode mass loading, capacity, and the areal capacity ratio of negative to positive electrodes (n/p ratio) in the full cell for the various over-lithiation conditions are given in Table 1.

The process of preparing the over-lithiated NMC electrodes is given in detail in the experimental section. In brief, NMC electrodes were lithiated to the pre-determined over-lithiation capacity by constructing half cells and discharging to a capacity limitation. The cells were then deconstructed, the cathode extracted, and paired versus a Si-graphite anode in a full cell. The discharge capacity and coulombic efficiency from full cell cycling are shown in Figure 7 for the baseline (no over-lithiation) and three over-lithiation conditions. Cycling was conducted between 3.0-4.1 V at C/20 for three formation cycles, followed by an initial hybrid pulse power characterization (HPPC) cycle, 92 aging cycles at C/3, a final HPPC cycle and lastly three C/20 diagnostic cycles. More details on the cycling protocol can be found in the experimental section. Representative voltage profiles for the first cycle are shown in Figure S7b. Without pre-lithiation of the cathode, the first discharge capacity at C/20 is 136.1 mAh g^{-1}_{NMC}. The capacity fades rapidly over 100 cycles, with 59 % capacity retention at C/20 after 100 cycles. The coulombic

efficiency is 97.9 % in the third cycle at C/20, slowly increases from 99.1 % to 99.4 % during the C/3 cycles, and is 98.3 % on cycle 100 at C/20. The slow improvement may in part be due to formation of a more robust SEI, but is also related to the decreasing capacity. Silicon particle expansion is a function of the lithiation capacity,[23,25,26,77–79] and therefore a lower capacity leads to less particle expansion and contraction, fewer lithium consuming passivation reactions and a higher coulombic efficiency.[80]

Over-lithiation of the cathode has clearly led to an improvement in the capacity and in some cases the capacity retention (Figure 7a). By compensating only for the first cycle irreversible capacity from lithium loss (23 mAh g^{-1}_{NMC}) the initial discharge capacity (145.2 mAh g^{-1}_{NMC}) is 9.1 mAh g^{-1}_{NMC} higher than without over-lithiation. The coulombic efficiency is slightly higher than the baseline across the first 40 cycles, although in the final 60 cycles it is equivalent to the cells without over-lithiation. After 100 cycles, the capacity increase over the baseline remains as it was initially at 9.1 mAh g^{-1}_{NMC} (89.0 mAh g^{-1}_{NMC}), with only a slight improvement to the capacity retention. The improvement for 46 and 70 mAh g^{-1}_{NMC} over-lithiation capacity is more pronounced due to the higher lithium inventory provided to the cell. In both of these cases, all the lithium on the cathode is delivered to the anode during the first charge. On discharge, the cathode fills before the anode relinquishes all the electrochemically available lithium, thereby leaving a reserve of lithium on the anode. This lithium can be released in subsequent cycles to compensate for the irreversible capacity occurring on each cycle. Since the capacity losses are lower after the first cycle, it takes many cycles for the lithium reserve to be exhausted. The rate of capacity fade and the coulombic efficiency are good indicators for when the lithium reserve is exhausted.[80] After over-lithiation to 46 mAh g^{-1}_{NMC} the capacity begins to fade faster and the coulombic efficiency begins to decrease from about cycle 40,

indicating the lithium reserve is nearly expended. This does not occur after over-lithiation to 70 mAh g^{-1}_{NMC} until approximately cycle 130. Consequently, the capacity retention after 100 cycles is 74 % and 89 % after over-lithiation to 46 and 70 mAh g^{-1}_{NMC}, respectively, a vast improvement upon the baseline case (59 %). After 200 cycles the capacity retention after over-lithiation to 70 mAh g^{-1}_{NMC} is 71 %, still much higher than the baseline case after 100 cycles.

Earlier we postulated that the capacity fade of the full cell would be determined by the lithium loses at the Si-graphite anode. To test this hypothesis the cathodes cycled in full cells (Figure 7) were extracted and rebuilt with a lithium metal counter/reference electrode. Cathodes without over-lithiation and with 20 mAh g^{-1}_{NMC} over-lithiation were extracted after 100 cycles, and those with 46 and 70 mAh g^{-1}_{NMC} were extracted after 200 cycles. The first discharge capacity in the rebuilt cell reveals the true capacity of the cycled cathode. By comparing this to the capacity of a cathode that has not been aged in a full cell, the cathode capacity retention can be determined. Without over-lithiation, $LiNMCO_2$ aged by 100 cycles in the full cell has 97.5 % capacity retention. Over-lithiation to 20 mAh g^{-1}_{NMC} shows 94 % retention. After 200 cycles in the full cell, over-lithiation to 46 and 70 mAh g^{-1}_{NMC} gives 92 % and 90 % retention, respectively. This data is summarized in Table S1. In each case, the full cell capacity loss (Figure 7) is greater than the cathode capacity loss (Table S1), verifying that the capacity fade in the $Li_{1+x}NMCO_2$/Si-graphite full cells is limited by the rate of active lithium loss at the Si-graphite anode rather than the capacity fade of the over-lithiated cathode.

While NMC over-lithiation is a viable way to introduce lithium inventory, one primary concern with using $Li_{1+x}NMCO_2$ as a lithium source and a cathode is that the structural and morphological changes induced as a result of over-lithiation may adversely affect the cell impedance. To examine this, the area specific impedance (ASI) on cycles 4 and 97 is plotted in

Figure S8 as a function of the open circuit voltage for baseline NMC (no over-lithiation) and after over-lithiation to varying degrees. The initial impedance after over-lithiation is 3.2 Ω cm^2 higher at ~3.6 V and up to 10 Ω cm^2 higher at lower and higher SOCs. However, the impedance rise (i.e. the difference between cycle 97 and cycle 4) is roughly equivalent for all conditions – data for the impedance rise at ~3.6 V is summarized in Table S2. In summary, while the over-lithiation process affects the initial impedance of the full cell, the impedance rise is minimally affected. Meanwhile, there is a significant gain in energy density and cyclability by increasing the lithium inventory in the cell by NMC over-lithiation.

Finally, we note that when a lithium reserve is present the coulombic efficiency increases quickly to 99.8 %, and remains above 99.6 % in the C/3 cycles. On cycle 100, the efficiency at C/20 is 99.5 % for the 70 mAh g^{-1}_{NMC} over-lithiation cells. It is important to further note that after the lithium reserve is exhausted the coulombic efficiency decreases to a value consistent with the baseline, no over-lithiation, condition. This implies that the inefficiencies of the Si-graphite electrode return to baseline levels irrespective of whether the lithium reserve is consumed after 1, 40 or 130 cycles. We surmise that there may be some critical content of lithium inventory necessary that must be added to the cell to fully "break-in" a Si-containing electrode, after which it will cycle with satisfactorily low irreversibility. The important questions are what this critical amount of lithium inventory is, and can the extra lithium be included in the cell in a practical way. For example, we know that the maximum amount of lithium in the cell can only be increased by either increasing the areal capacity (laminate thickness) of the anode, or decreasing the areal capacity of the cathode; in both cases increasing the n/p ratio. Either allows more over-lithiation capacity on the cathode without risking lithium plating on the anode in the

first charge. The drawback is that the energy density of the cell is lowered, possibly losing any gain from using silicon in place of graphite.

Conclusions

In this study, we show over-lithiated $Li_{1+x}NMCO_2$ to be an effective lithium source *and* cathode material when paired with a Si-containing anode in a LIB full cell. The "extra" lithium (x) compensates for the irreversible capacity loss due to SEI formation at the silicon-graphite electrode and allows the "original" lithium on the NMC cathode to be cycled reversibly to give higher capacity and better capacity retention. Unlike many other approaches of pre-lithiation, direct over-lithiation of the cathode does not add deadweight to the cell in the form of inactive phases and thus does not adversely impact the energy density. We show that $Li_{1+x}NMCO_2$ can be formed both chemically, via a reaction between NMC and lithium naphthalide, and electrochemically. To compensate for the irreversible capacity of a Si-containing electrode only low levels of lithiation are required, and half cell electrochemical tests demonstrate that such levels of lithiation (up to 60 mAh g^{-1}_{NMC}) give capacity retention on par with the baseline NMC while minimally affecting the capacity. To investigate the limits of this system, higher amounts of lithiation were also explored in half cells but these lead to more rapid capacity loss. Ex situ XAS after over-lithiation to 1.1 V vs Li/Li^+ (123 mAh g^{-1}_{NMC}) reveals that Ni, Co, and Mn are each partially reduced relative to their starting oxidation states, with the formation of Jahn-Teller active Mn^{3+} and Co^{2+} giving rise to a strong increase in local disorder. Bulk structure characterization by in situ synchrotron XRD reveals that the poorer electrochemical performance of highly over-lithiated NMCs is also linked to hysteresis in the structural evolution during over-lithiation and delithiation, but also due to a "buckling" of the layered structure leading to a greater degree of lithium removal in the charged state. However, we illustrate that both these

difficulties can be avoided by low-to-moderate over-lithiation. Using $Li_{1+x}NMCO_2$ cathodes in full cells with Si-graphite anodes greatly improves the capacity, capacity retention, and extends cell life without affecting the cell impedance rise. The highest over-lithiation capacity tested in the full cell delivers 67 % more capacity after 100 cycles and greatly increases the useable silicon capacity. The average coulombic efficiency is increased by 0.52 % by virtue of the lithium reserve on the Si-graphite anode (sent there from the cathode on the first charge of the cell) that adds lithium ions to the cycleable inventory to compensate for the ongoing irreversible lithium trapping reactions. Overall, the over-lithiation method demonstrated in this work introduces a new approach to increase the lithium inventory and maximize the energy density of LIBs with NMC cathodes and next-generation anodes. This method is demonstrated for NMC with 50 % nickel content, but is expected to be applicable to the wider family of layered transition metal oxides and is therefore relevant for next-generation LIB chemistries with high-energy nickel-rich NMC cathodes, which are on the roadmap for most automotive companies producing EVs. When coupled with new advances that stabilize the silicon surface, this novel pre-lithiation strategy has the potential to enable the widespread application of next-generation LIBs.

Author contributions

W.M.D. Conceptualization, Methodology, Formal analysis, Investigation, Writing - Original Draft; **S.K.** Formal analysis, Investigation; **Q.L.** Investigation; **S.E.T.** Resources; **A.R.D.** Investigation; **Y.R.** Resources; **Z.Z.** Supervision; **T.T.F.** Formal analysis, Supervision; **C.S.J.** Conceptualization, Writing - Review & Editing, Supervision.

Acknowledgements

Support from the Vehicle Technologies Program, Hybrid and Electric Systems, in particular, David Howell, Tien Duong, Peter Faguy, and Brian Cunningham at the U.S. Department of Energy (DOE), Office of Energy Efficiency and Renewable Energy is gratefully acknowledged. This manuscript has been created by UChicago Argonne, LLC, Operator of Argonne National Laboratory (a DOE Office of Science laboratory) under Contract No. DE-AC02-06CH11357. This research used resources of the Advanced Photon Source, a U.S. Department of Energy (DOE) Office of Science User Facility operated for the DOE Office of Science by Argonne National Laboratory under Contract No. DE-AC02-06CH11357. The authors acknowledge Dean Bass for assistance obtaining the ICP-MS data.

Conflicts of interest

There are no conflicts to declare.

References

1 N. Yabuuchi and T. Ohzuku, *J. Power Sources*, 2005, **146**, 636–639.
2 K. Amine, Z. Chen, Z. Zhang, J. Liu, W. Lu, Y. Qin, J. Lu, L. Curtis and Y. K. Sun, *J. Mater. Chem.*, 2011, **21**, 17754–17759.
3 H. Zheng, Q. Sun, G. Liu, X. Song and V. S. Battaglia, *J. Power Sources*, 2012, **207**, 134–140.
4 D. R. Gallus, R. Schmitz, R. Wagner, B. Hoffmann, S. Nowak, I. Cekic-Laskovic, R. W. Schmitz and M. Winter, *Electrochim. Acta*, 2014, **134**, 393–398.
5 I. Buchberger, S. Seidlmayer, A. Pokharel, M. Piana, J. Hattendorff, P. Kudejova, R. Gilles and H. A. Gasteiger, *J. Electrochem. Soc.*, 2015, **162**, A2737–A2746.
6 N. V. Faenza, Z. W. Lebens-Higgins, P. Mukherjee, S. Sallis, N. Pereira, F. Badway, A. Halajko, G. Ceder, F. Cosandey, L. F. J. Piper and G. G. Amatucci, *Langmuir*, 2017, **33**, 9333–9353.
7 Y. Itou and Y. Ukyo, in *Journal of Power Sources*, Elsevier, 2005, vol. 146, pp. 39–44.
8 Y. Makimura, S. Zheng, Y. Ikuhara and Y. Ukyo, *J. Electrochem. Soc.*, 2012, **159**, A1070–A1073.
9 H. Liu, M. Wolf, K. Karki, Y. S. Yu, E. A. Stach, J. Cabana, K. W. Chapman and P. J. Chupas, *Nano Lett.*, 2017, **17**, 3452–3457.
10 F. Schipper, E. M. Erickson, C. Erk, J.-Y. Shin, F. F. Chesneau and D. Aurbach, *J. Electrochem. Soc.*, 2017, **164**, A6220–A6228.
11 Z. W. Lebens-Higgins, S. Sallis, N. V. Faenza, F. Badway, N. Pereira, D. M. Halat, M. Wahila, C. Schlueter, T. L. Lee, W. Yang, C. P. Grey, G. G. Amatucci and L. F. J. Piper, *Chem. Mater.*, 2018, **30**, 958–969.

12 R. Jung, M. Metzger, F. Maglia, C. Stinner and H. A. Gasteiger, *J. Electrochem. Soc.*, 2017, **164**, A1361–A1377.
13 R. Jung, M. Metzger, F. Maglia, C. Stinner and H. A. Gasteiger, *J. Phys. Chem. Lett.*, 2017, **8**, 4820–4825.
14 D. P. Abraham, R. D. Twesten, M. Balasubramanian, J. Kropf, D. Fischer, J. McBreen, I. Petrov and K. Amine, *J. Electrochem. Soc.*, 2003, **150**, A1450.
15 S. K. Jung, H. Gwon, J. Hong, K. Y. Park, D. H. Seo, H. Kim, J. Hyun, W. Yang and K. Kang, *Adv. Energy Mater.*, 2014, **4**, 1300787.
16 F. Lin, I. M. Markus, D. Nordlund, T. C. Weng, M. D. Asta, H. L. Xin and M. M. Doeff, *Nat. Commun.*, 2014, **5**, 3529.
17 R. Petibon, L. Madec, D. W. Abarbanel and J. R. Dahn, *J. Power Sources*, 2015, **300**, 419–429.
18 K. J. Nelson, D. W. Abarbanel, J. Xia, Z. Lu and J. R. Dahn, *J. Electrochem. Soc.*, 2016, **163**, A272–A280.
19 J. Wandt, A. T. S. Freiberg, A. Ogrodnik and H. A. Gasteiger, *Mater. Today*, 2018, **21**, 825–833.
20 J. A. Gilbert, I. A. Shkrob and D. P. Abraham, *J. Electrochem. Soc.*, 2017, **164**, A389–A399.
21 J. Wandt, A. Freiberg, R. Thomas, Y. Gorlin, A. Siebel, R. Jung, H. A. Gasteiger and M. Tromp, *J. Mater. Chem. A*, 2016, **4**, 18300–18305.
22 X. Su, Q. Wu, J. Li, X. Xiao, A. Lott, W. Lu, B. W. Sheldon and J. Wu, *Adv. Energy Mater.*, 2014, **4**, 1300882.
23 L. Y. Beaulieu, K. W. Eberman, R. L. Turner, L. J. Krause and J. R. Dahna, *Electrochem. Solid-State Lett.*, 2001, **4**, A137.
24 A. L. Michan, G. Divitini, A. J. Pell, M. Leskes, C. Ducati and C. P. Grey, *J. Am. Chem. Soc.*, 2016, **138**, 7918–7931.
25 Y. Oumellal, N. Delpuech, D. Mazouzi, N. Dupré, J. Gaubicher, P. Moreau, P. Soudan, B. Lestriez and D. Guyomard, *J. Mater. Chem.*, 2011, **21**, 6201–6208.
26 E. Radvanyi, W. Porcher, E. De Vito, A. Montani, S. Franger and S. Jouanneau Si Larbi, *Phys. Chem. Chem. Phys.*, 2014, **16**, 17142–17153.
27 K. Xu, *Chem. Rev.*, 2004, **104**, 4303–4418.
28 P. Verma, P. Maire and P. Novák, *Electrochim. Acta*, 2010, 55, 6332–6341.
29 F. Holtstiege, A. Wilken, M. Winter and T. Placke, *Phys. Chem. Chem. Phys.*, 2017, **19**, 25905–25918.
30 V. Aravindan, Y.-S. Lee and S. Madhavi, *Adv. Energy Mater.*, 2017, **7**, 1602607.
31 Z. Wang, Y. Fu, Z. Zhang, S. Yuan, K. Amine, V. Battaglia and G. Liu, *J. Power Sources*, 2014, **260**, 57–61.
32 M. W. Forney, M. J. Ganter, J. W. Staub, R. D. Ridgley and B. J. Landi, *Nano Lett.*, 2013, **13**, 4158–4163.
33 C. R. Jarvis, M. J. Lain, M. V. Yakovleva and Y. Gao, *J. Power Sources*, 2006, **162**, 800–802.
34 N. Liu, L. Hu, M. T. McDowell, A. Jackson and Y. Cui, *ACS Nano*, 2011, **5**, 6487–6493.
35 H. J. Kim, S. Choi, S. J. Lee, M. W. Seo, J. G. Lee, E. Deniz, Y. J. Lee, E. K. Kim and J. W. Choi, *Nano Lett.*, 2016, **16**, 282–288.
36 Z. Cao, P. Xu, H. Zhai, S. Du, J. Mandal, M. Dontigny, K. Zaghib and Y. Yang, *Nano Lett.*, 2016, **16**, 7235–7240.

37 H. Zhou, X. Wang and D. Chen, *ChemSusChem*, 2015, **8**, 2737–2744.
38 Y. Sun, H. W. Lee, Z. W. Seh, N. Liu, J. Sun, Y. Li and Y. Cui, *Nat. Energy*, 2016, **1**, 1–7.
39 K. Park, B.-C. Yu and J. B. Goodenough, *Adv. Energy Mater.*, 2016, **6**, 1502534.
40 Y. Sun, H.-W. Lee, Z. W. Seh, G. Zheng, J. Sun, Y. Li and Y. Cui, *Adv. Energy Mater.*, 2016, **6**, 1600154.
41 Y. Sun, H. W. Lee, G. Zheng, Z. W. Seh, J. Sun, Y. Li and Y. Cui, *Nano Lett.*, 2016, **16**, 1497–1501.
42 A. Abouimrane, Y. Cui, Z. Chen, I. Belharouak, H. B. Yahia, H. Wu, R. Assary, L. A. Curtiss and K. Amine, *Nano Energy*, 2016, **27**, 196–201.
43 X. Su, C. Lin, X. Wang, V. A. Maroni, Y. Ren, C. S. Johnson and W. Lu, *J. Power Sources*, 2016, **324**, 150–157.
44 P. Jezowski, K. Fic, O. Crosnier, T. Brousse and F. Béguin, *J. Mater. Chem. A*, 2016, **4**, 12609–12615.
45 Y. Bie, J. Yang, J. Wang, J. Zhou and Y. Nuli, *Chem. Commun.*, 2017, **53**, 8324–8327.
46 S. Solchenbach, M. Wetjen, D. Pritzl, K. U. Schwenke and H. A. Gasteiger, *J. Electrochem. Soc.*, 2018, **165**, A512–A524.
47 W. M. Dose, C. Villa, X. Hu, A. R. Dunlop, M. J. Piernas-Muñoz, V. A. Maroni, S. E. Trask, I. Bloom, V. Dravid and C. S. Johnson, *J. Electrochem. Soc.*, 2020, **167**, 160543.
48 Z. Moorhead-Rosenberg, E. Allcorn and A. Manthiram, *Chem. Mater.*, 2014, **26**, 5905–5913.
49 M. Mancini, P. Axmann, G. Gabrielli, M. Kinyanjui, U. Kaiser and M. Wohlfahrt-Mehrens, *ChemSusChem*, 2016, **9**, 1843–1849.
50 G. Gabrielli, M. Marinaro, M. Mancini, P. Axmann and M. Wohlfahrt-Mehrens, *J. Power Sources*, 2017, **351**, 35–44.
51 M. Mancini, G. Gabrielli, P. Axmann and M. Wohlfahrt-Mehrens, *J. Electrochem. Soc.*, 2017, **164**, A6229–A6235.
52 W. M. Dose, J. Blauwkamp, M. J. Piernas-Muñoz, I. Bloom, X. Rui, R. F. Klie, P. Senguttuvan and C. S. Johnson, *ACS Appl. Energy Mater.*, 2019, **2**, 5019–5028.
53 J. M. Tarascon and D. Guyomard, *J. Electrochem. Soc.*, 1991, **138**, 2864–2868.
54 W. Li, W. R. McKinnon and J. R. Dahn, *J. Electrochem. Soc.*, 1994, **141**, 2310–2316.
55 W. I. F. David, M. M. Thackeray, L. A. De Picciotto and J. B. Goodenough, *J. Solid State Chem.*, 1987, **67**, 316–323.
56 Y. J. Lee, F. Wang and C. P. Grey, *J. Am. Chem. Soc.*, 1998, **120**, 12601–12613.
57 C. S. Johnson, J. S. Kim, A. Jeremy Kropf, A. J. Kahaian, J. T. Vaughey and M. M. Thackeray, *Electrochem. commun.*, 2002, **4**, 492–498.
58 C. S. Johnson, J. S. Kim, A. J. Kropf, A. J. Kahaian, J. T. Vaughey, L. M. L. Fransson, K. Edström and M. M. Thackeray, *Chem. Mater.*, 2003, **15**, 2313–2322.
59 M. G. S. R. David, W. I. F.; Goodenough, J. B.; Thackeray, M. M.; Thomas, *Rev. Chem. Miner.*, 1983, **20**, 636–642.
60 J. R. Dahn, U. von Sacken and C. A. Michal, *Solid State Ionics*, 1990, **44**, 87–97.
61 S. H. Kang, D. P. Abraham, W. S. Yoon, K. W. Nam and X. Q. Yang, *Electrochim. Acta*, 2008, **54**, 684–689.
62 S. H. Kang, W. S. Yoon, K. W. Nam, X. Q. Yang and D. P. Abraham, *J. Mater. Sci.*, 2008, **43**, 4701–4706.
63 R. Robert and P. Novák, *Chem. Mater.*, 2018, **30**, 1907–1911.

64 K. Qian, Y. Li, Y. B. He, D. Liu, Y. Zheng, D. Luo, B. Li and F. Kang, *RSC Adv.*, 2016, **6**, 76897–76904.

65 D. Dees, E. Gunen, D. Abraham, A. Jansen and J. Prakash, *J. Electrochem. Soc.*, 2008, **155**, A603.

66 B. Ravel and M. Newville, *J. Synchrotron Radiat.*, 2005, **12**, 537–541.

67 B. H. Toby and R. B. Von Dreele, *J. Appl. Crystallogr.*, 2013, **46**, 544–549.

68 K. Märker, P. J. Reeves, C. Xu, K. J. Griffith and C. P. Grey, *Chem. Mater.*, 2019, **31**, 2545–2554.

69 A. Grenier, P. J. Reeves, H. Liu, I. D. Seymour, K. Märker, K. M. Wiaderek, P. J. Chupas, C. P. Grey and K. W. Chapman, *J. Am. Chem. Soc.*, 2020, **142**, 7001–7011.

70 J. Kasnatscheew, U. Rodehorst, B. Streipert, S. Wiemers-Meyer, R. Jakelski, R. Wagner, I. C. Laskovic and M. Winter, *J. Electrochem. Soc.*, 2016, **163**, A2943–A2950.

71 I. J. Davidson, J. E. Greedan, U. Von Sacken, C. A. Michal and W. R. McKinnon, *J. Solid State Chem.*, 1993, **105**, 410–416.

72 G. G. Amatucci, J. M. Tarascon and L. C. Klein, *J. Electrochem. Soc.*, 1996, **143**, 1114–1123.

73 S. C. Yin, Y. H. Rho, I. Swainson and L. F. Nazar, *Chem. Mater.*, 2006, **18**, 1901–1910.

74 A. O. Kondrakov, H. Geßwein, K. Galdina, L. De Biasi, V. Meded, E. O. Filatova, G. Schumacher, W. Wenzel, P. Hartmann, T. Brezesinski and J. Janek, *J. Phys. Chem. C*, 2017, **121**, 24381–24388.

75 K. Kang and G. Ceder, *Phys. Rev. B - Condens. Matter Mater. Phys.*, 2006, **74**, 094105.

76 K. Kang, Y. S. Meng, J. Bréger, C. P. Grey and G. Ceder, *Science*, 2006, **311**, 977–980.

77 J. O. Besenhard, J. Yang and M. Winter, *J. Power Sources*, 1997, **68**, 87–90.

78 M. N. Obrovac and V. L. Chevrier, *Chem. Rev.*, 2014, **114**, 11444–11502.

79 M. N. Obrovac and L. J. Krause, *J. Electrochem. Soc.*, 2007, **154**, A103.

80 W. M. Dose, V. A. Maroni, M. J. Piernas-Muñoz, S. E. Trask, I. Bloom and C. S. Johnson, *J. Electrochem. Soc.*, 2018, **165**, A2389–A2396.

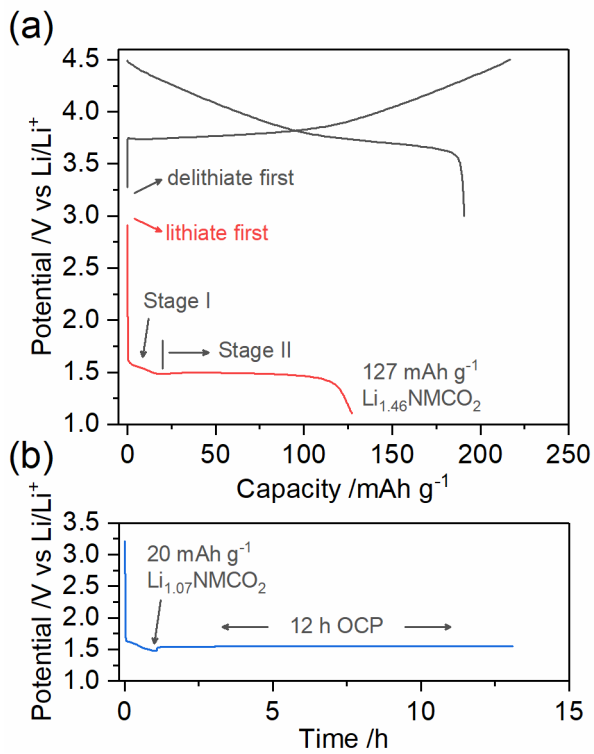

Figure 1. (a) Illustration of the over-lithiation capability of a layered $LiNi_{0.5}Mn_{0.3}Co_{0.2}O_2$ cathode. Potential profiles of $LiNi_{0.5}Mn_{0.3}Co_{0.2}O_2$ for galvanostatic lithiation (red) compared to the standard delithiation-lithiation (black) versus lithium metal at a rate of C/10. In (b) the potential relaxation after a 20 mAh g^{-1}_{NCM} over-lithiation is shown.

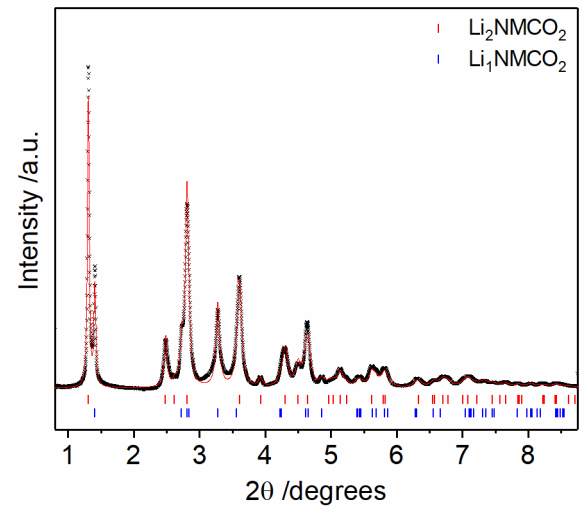

Figure 2. Rietveld refined fit of synchrotron X-ray diffraction data of chemically lithiated $Li_{1+x}Ni_{0.5}Mn_{0.3}Co_{0.2}O_2$ (wavelength 0.1173 Å). Data is shown as black crosses and the fit as a red line. Reflection markers for the Li_2NMCO_2 (P-3m_1 space group) and Li_1NMCO_2 (R-3m space group) phases are shown in red and blue, respectively. Li_1NMCO_2: a = 2.8894(7) Å, c = 14.323(2) Å, phase fraction = 17.4(1) %. Li_2NMCO_2: a = 3.1239(4) Å, c = 5.1325(4) Å, phase fraction = 82.6(4) %. wR = 5.87 % and goodness of fit = 3.15.

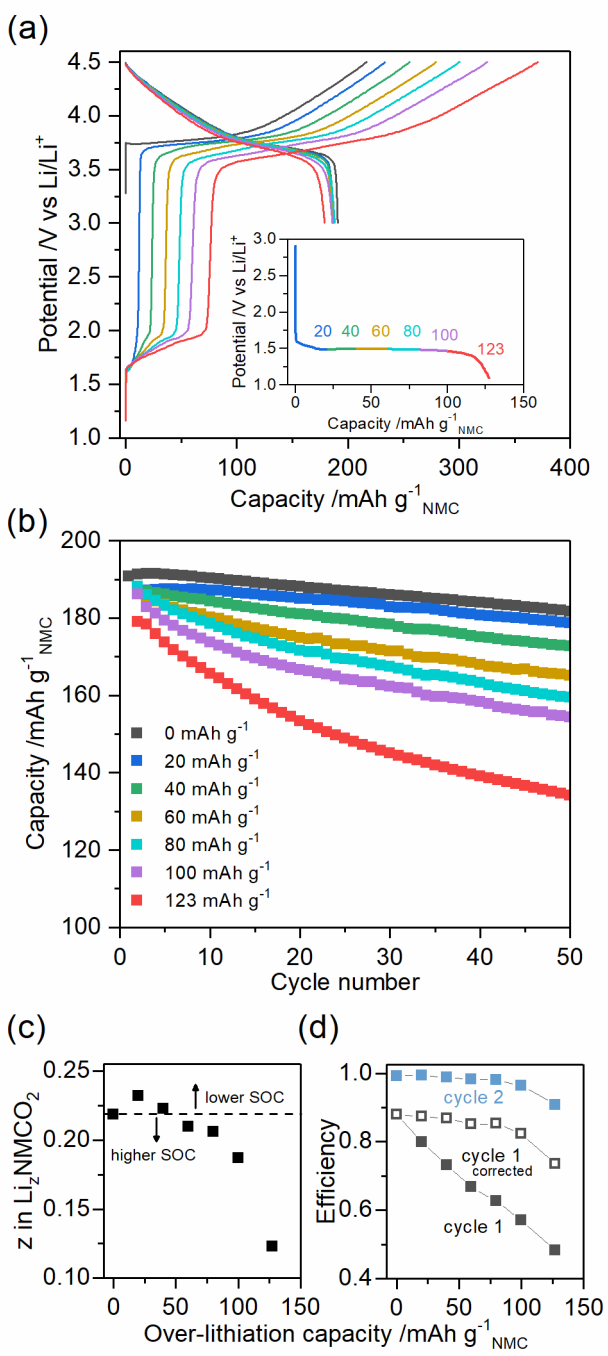

Figure 3. (a) Potential profiles for $LiNi_{0.5}Mn_{0.3}Co_{0.2}O_2$ during over-lithiation to various extents (inset) and the following cycle between 3.0 and 4.5 V vs Li/Li^+. (b) Discharge capacity over 50 cycles for $LiNi_{0.5}Mn_{0.3}Co_{0.2}O_2$ without over-lithiation (black data) and with over-lithiation to various amounts (colored data). (c) Lithium content (z in $Li_zMn_{0.3}Ni_{0.5}Co_{0.2}O_2$) in the first charged state, and (d) cycle efficiency as a function of over-lithiation capacity. In (d) the cycle number is indicated. The closed and open black data points show the measured and corrected first cycle efficiency, respectively. The corrected efficiency is calculated using $efficiency_{corrected} = Q_d / (Q_c - Q_o)$, where Q is the capacity, and d, c, and o represent discharge, charge and over-lithiation, respectively.

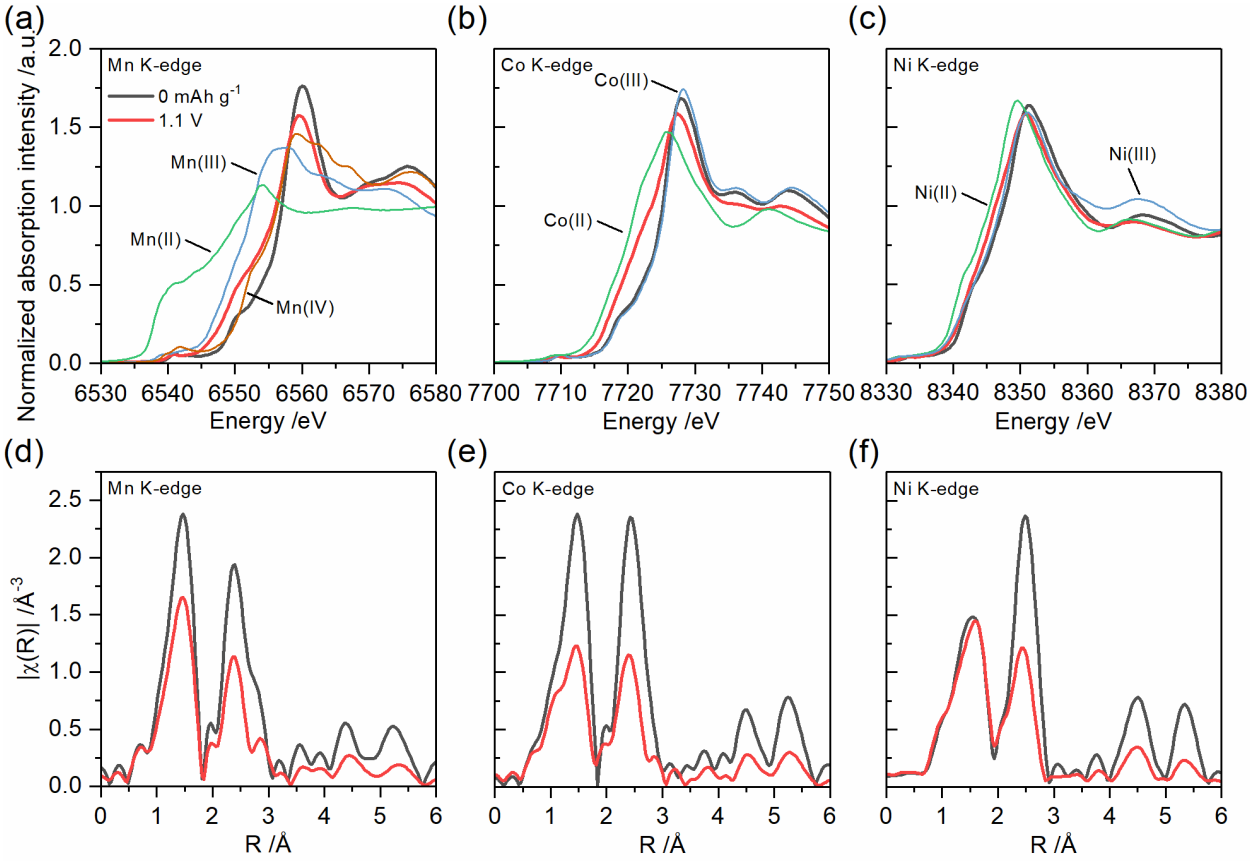

Figure 4. (a) Mn, (b) Co, and (c) Ni K-edge X-ray absorption near edge structure of pristine (black) and over-lithiated $Li_{1+x}Mn_{0.3}Ni_{0.5}Co_{0.2}O_2$ (red) together with relevant standards as labelled. Extended X-ray absorption fine structure of (d) Mn, (e) Co, and (f) Ni.

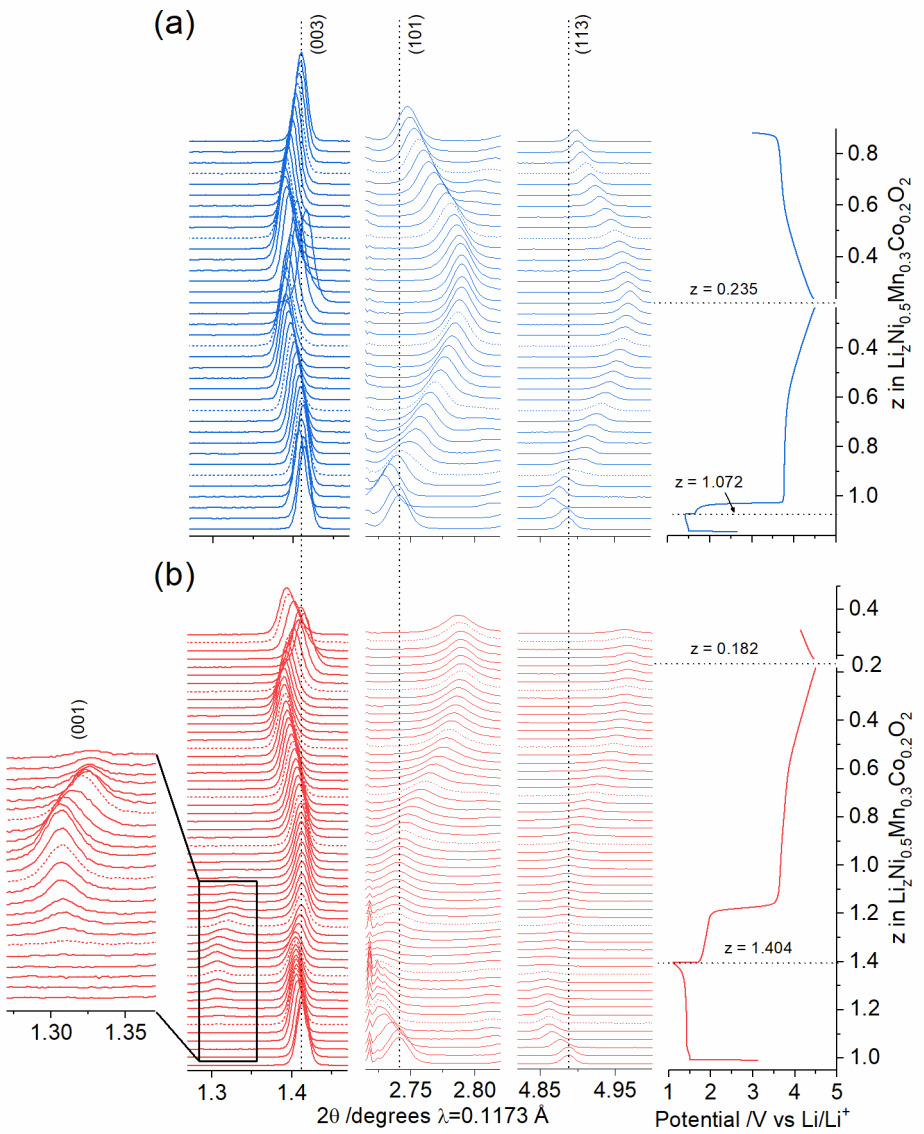

Figure 5. Evolution of selected peaks from in situ X-ray diffraction data together with the potential profiles for the over-lithiation and subsequent charge-discharge cycle of $LiNi_{0.5}Co_{0.2}Mn_{0.3}O_2$. Over-lithiation step to a 20 mAh g^{-1} limit (a), and 1.1 V vs Li/Li^+ limit (112 mAh g^{-1}, b) are shown. The plot to the left of (b) shows the zoomed region indicated by a rectangle, and tracks the position of the weak (001) reflection from the Li_2NCMO_2 phase.

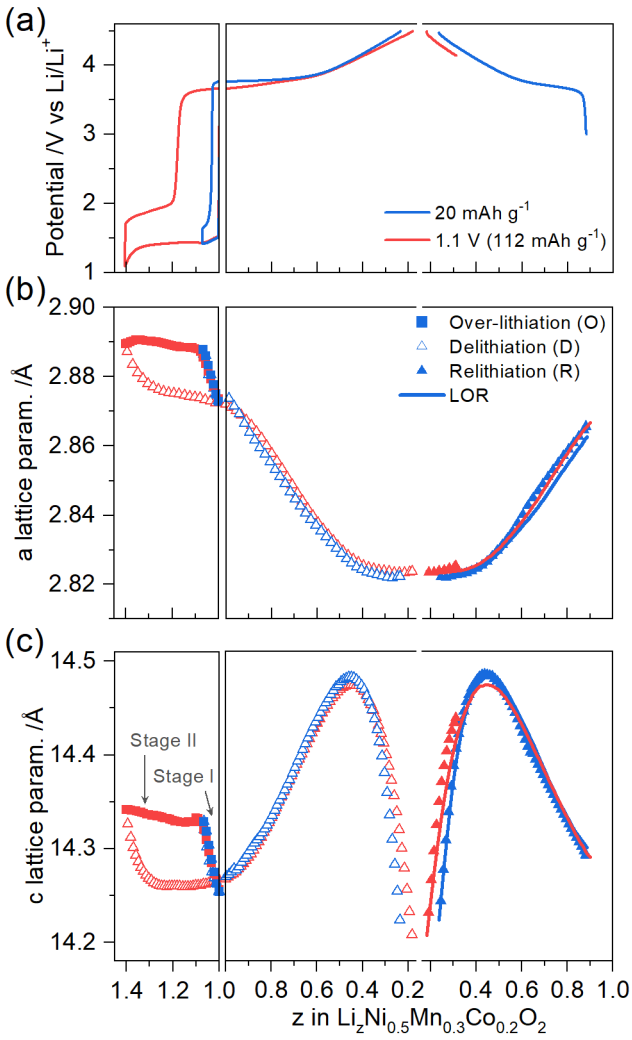

Figure 6. Potential profiles (a) and a and c lattice parameters (b) and (c), respectively, obtained from Rietveld refinements during over-lithiation (O), delithiation (D) and relithiation (R). The estimated errors are within the data markers. A solid line is shown over the relithiation data showing the hypothetical pathway without structural hysteresis, labelled the line of reversibility (LOR).

Table 1. Electrode properties of the $Li_{1+x}Ni_{0.5}Mn_{0.3}Co_{0.2}O_2$ cathodes and Si-graphite anode used in full cells. Practical capacities for the $LiNi_{0.5}Mn_{0.3}Co_{0.2}O_2$ and Si-graphite electrodes were taken as 180 mAh g^{-1}_{NCM} and 1024 mAh $g^{-1}_{Si\text{-}graphite}$ and were used to calculate the electrode areal capacities. The numbers in the brackets represent the deviation between the electrodes employed in this work.

Over-lithiation capacity mAh g^{-1}_{NMC}	x in $Li_{1+x}NMCO_2$	$Li_{1+x}NMCO_2$ cathode		Si-graphite anode		n/p
		mg cm^{-2}	mAh cm^{-2}	mg cm^{-2}	mAh cm^{-2}	
0	0	10.2(2)	1.86(3)	2.8(2)	2.80(1)	1.51(3)
23	0.08		2.19(1)			1.34(3)
46	0.17		2.43(1)			1.20(2)
70	0.25		2.67(2)			1.09(2)

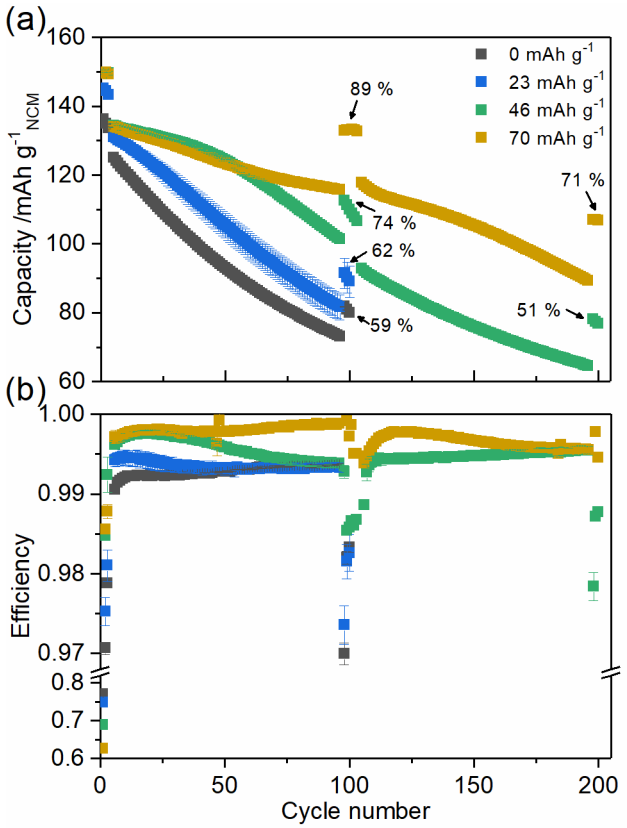

Figure 7. Specific discharge capacity (a) and coulombic efficiency (b) of $Li_{1+x}Ni_{0.5}Mn_{0.3}Co_{0.2}O_2$/Si-graphite cells with varying degrees of electrochemical over-lithiation during cycling between 3.0-4.1 V and at 30 °C. The first and last three cycles of each set of 100 cycles were performed at C/20, cycle 4 and 97 are HPPC cycles, and cycles 5-96 were performed at C/3. Capacity retention at cycle 100 and 200 (compared to cycle 2) are indicated. Results are averaged over two cells and the error bars (in many cases smaller than the symbols) represent the variation between the cells.